Spectrum of Engineering Sciences
ISSN (e) 3007-3138 (p) 3007-312X Volume 3, Issue 10, 2025

SYNTHESIS AND CHARACTERIZATION OF MANGANESE (MN) DOPED TUNGSTEN OXIDE (WO_3) HYDROGELS FOR ENHANCED PHOTOCATALYTIC APPLICATION IN WASTEWATER TREATMENT

**Neelam Shahadat[*1], Shaheena Anjum[2], Hafza Ayesha Umar[3], Zakir Ullah[4]
Raja Muhammad Jawad Naveed[5], Muhammad Saud Ahmed[6]**

[*1]*Department of Chemistry, University of Agriculture, Faisalabad, Pakistan*
[2]*Department of Chemistry, Riphah International University, Faisalabad, Pakistan.*
[3]*Department of Chemistry, Government College University, Faisalabad, Pakistan.*
[4]*Institute of Chemical Sciences, University of Swat, Swat, Pakistan.*
[5]*Department of Chemistry, University of Gujrat, Gujrat, Pakistan*
[6]*Department of Chemistry, University of Education, Lahore, Pakistan*

[*1]malikneelo82@gmail.com, [2]shaheenaharoon4@gmail.com, [3]ibraheemk145@gmail.com,
[4]zakirchemist020@gmail.com, [5]rajajawadnaveed28@gmail.com, [6]msaudahmed171@gmail.com

DOI:https://doi.org/10.5281/zenodo.17374605

Keywords
Manganese-doped tungsten oxide, hydrogel composites, photocatalysis, wastewater treatment, hydrothermal synthesis, dye degradation.

Article History
Received: 28 August 2025
Accepted: 05 October 2025
Published: 17 October 2025

Corresponding Author: *
Neelam Shahadat

Abstract

Water contamination by dyes, heavy metals, and agricultural effluents presents an urgent global challenge requiring sustainable treatment solutions. Semiconductor photocatalysis has emerged as a promising eco-friendly approach; however, limitations such as wide band gaps and rapid electron–hole recombination hinder its efficiency. This study presents the synthesis and characterization of Mn-doped WO_3 nanoparticles and Mn-WO_3/$(C_{12}H_{14}CaO_{12})_n$ hydrogel composites for efficient photocatalytic degradation of organic pollutants in wastewater. The materials were prepared via a hydrothermal route, with Mn doping narrowing the WO_3 bandgap from 2.91 to 2.80 eV, enhancing visible-light absorption. Characterization techniques, including FTIR, XRD, and UV-Vis DRS, confirmed successful doping and hydrogel incorporation. Photocatalytic activity was evaluated against methylene blue under solar irradiation, with optimized parameters of pH 3, catalyst concentration (15 mg/100 mL for composites), and oxidant dose (11 mM H_2O_2). The Mn-WO_3/hydrogel composites achieved >92% degradation within 100 minutes, outperforming pure Mn-WO_3. Radical scavenging experiments identified hydroxyl radicals as the primary reactive species. The composites exhibited good reusability, maintaining ~82% efficiency after three cycles. Kinetic modeling revealed pseudo-first-order behavior, while response surface methodology (RSM) validated the robustness of the composites under varying pollutant concentrations. The dual-function system of adsorption and photocatalytic degradation offered by Mn-doped WO_3 hydrogels provides a cost-effective, recyclable, and solar-driven strategy for wastewater remediation, with potential applications in environmental purification, antimicrobial treatments, sensing, and energy storage.

INTRODUCTION

Water is the most vital natural resource for supporting life and driving economic growth, yet its shortage and pollution have become significant global issues. The rising population, swift industrial growth, and uncontrolled release of untreated waste into natural water sources have put tremendous pressure on existing water supplies (Baggio, Qadir, and Smakhtin (2021). At present, significant efforts are being directed toward discovering sustainable strategies for augmenting water resources and enhancing treatment methods, with wastewater recycling emerging as a pivotal global goal. Despite the advanced biological and chemical techniques employed by contemporary wastewater treatment facilities, many stubborn contaminants remain unresolved (Silva, 2023). This has led to a growing interest in developing durable and eco-friendly technologies to guarantee a consistent supply of clean water (Pandey, 2025).

Waterborne infections continue to pose a significant global threat, with diarrheal diseases claiming the lives of nearly 2 million individuals each year, predominantly affecting children under five years old (WHO, 2018). In Pakistan, approximately 60 million people are at risk due to elevated arsenic levels in their drinking water, marking the largest recorded instance of mass arsenic poisoning globally (Guglielmi, 2017). Long-term arsenic exposure can lead to skin lesions, cancer, cardiovascular issues, diabetes, neurological damage, and harm to essential organs like the kidneys, liver, and bladder (Archana, Kanakalakshmi, Nithya, Kaarunya, & Renugadevi, 2025) Besides heavy metals, organic dyes are another group of persistent pollutants. Effluents from the textile industry, laden with synthetic dyes, significantly deteriorate water quality by raising biochemical and chemical oxygen demand (BOD and COD), impeding photosynthesis, and infiltrating the food chain. These dyes, noted for their persistence, mutagenic properties, and carcinogenic potential, present a substantial ecological and public health concern (Lellis, Fávaro-Polonio, Pamphile, & Polonio, 2019)

The textile industry is recognized globally as one of the most water-demanding and environmentally harmful sectors, producing wastewater that not only tarnishes the visual quality of water bodies but also disrupts ecosystems and accumulates in aquatic organisms (Dutta et al., 2024) (Sharma, Sharma, & Soni, 2021). Traditional methods for treating wastewater, such as coagulation, precipitation, ion-exchange, and activated carbon adsorption, are plagued by significant drawbacks, including high energy demands, incomplete pollutant removal, the creation of secondary pollutants, and complex operational requirements (Fernandes, Ramísio, & Puga, 2024). As a result, there is a growing interest in exploring advanced treatment strategies. Among these, Advanced Oxidation Processes (AOPs) in combination with biological methods have emerged as promising solutions (Ponnusami et al., 2023) (Bermúdez, Pascual, Martínez, & Poyatos Capilla, 2021). AOPs rely on the in situ generation of highly reactive radicals, such as hydroxyl and superoxide radicals, which can effectively break down persistent organic pollutants and dyes into harmless end-products like CO_2 and H_2O (Oller, Malato, & Sánchez-Pérez, 2011). These radicals are more reactive and efficient in mineralizing contaminants compared to conventional oxidants like hydrogen peroxide. Moreover, heterogeneous photocatalysis, which employs semiconductor-based materials, has gained popularity as a sustainable and cost-effective water treatment method (Lam, Sin, Abdullah, & Mohamed, 2012). This process utilizes solar energy to activate photocatalysts, generating electron–hole pairs that promote the formation of reactive oxygen species (ROS) capable of degrading pollutants. Photocatalysis often faces limitations due to large band gaps and the recombination of photogenerated electron–hole pairs. To overcome these obstacles, researchers have explored doping techniques and the creation of nanocomposites that merge the advantages of semiconductor nanoparticles with the adsorption properties of porous support materials. In this regard, hydrogels have been identified as highly effective and adaptable materials.

Hydrogels are three-dimensional polymer networks that are cross-linked, featuring excellent water retention, high porosity, and the ability to modify functional groups (Mu, Liu, Chen, Wang, & Yang, 2020). Their hydrophilic properties and adjustable chemical makeup make them perfect for absorbing heavy metals, dyes, and other contaminants from

wastewater (Nawaz, Zahid, Rehman, Mansha, & Hussain, 2023). Additionally, hydrogels are advantageous due to their recyclability and reusability, which makes them both environmentally friendly and cost-effective (Zhou, Guo, Zhao, & Yu, 2019). Recent advancements in hybrid hydrogels, which integrate nanoparticles like metal oxides or doped semiconductors, have greatly improved their adsorption, photocatalytic, and antimicrobial properties (Zhang et al., 2022). Nanoparticles, especially semiconductors, are crucial in heterogeneous photocatalysis because of their high surface-to-volume ratio, adjustable band gaps, and distinctive electronic characteristics (Gisbertz & Pieber, 2020). Doping WO_3 with transition metals such as manganese (Mn) can further boost its photocatalytic performance by minimizing electron-hole recombination and enhancing visible light absorption (Sayed Abhudhahir & Kandasamy, 2015). Tungsten oxide (WO_3) has attracted significant attention due to its promising photocatalytic activity(Al-Rasheed, 2005). Its band gap, which lies between 2.6 and 2.8 eV, allows WO_3 to absorb visible light more effectively than TiO_2 (Hoffmann, Martin, Choi, & Bahnemann, 1995). The valence band potential of WO_3, ranging from 2.7 to 3.44 eV, supports the formation of highly oxidative holes, making it particularly effective in degrading organic pollutants (S. Chen, Hu, Meng, & Fu, 2014).Additionally, WO_3 is known for being abundant, non-toxic, chemically stable, and environmentally safe (Nishimoto, Mano, Kameshima, & Miyake, 2010).However, its application is limited by the quick recombination of photogenerated electron hole pairs and a low conduction band edge, which hampers electron transfer and reduces the efficiency of reactive oxygen species production (Thangavel, Elayaperumal, & Venugopal, 2012). As a result, a significant amount of effort has been put into modifying the electrical structure of the semiconductor WO3 in order to improve the performance of its photocatalytic capabilities. To mitigate these issues, researchers have extensively explored metal doping to adjust the electronic structure of WO_3. Manganese (Mn) doping, specifically, introduces impurity levels within the band gap, thereby lowering the band gap energy and improving visible-light absorption(Hung et al., 2016).Mn ions also function as charge-trapping sites, which slow down recombination and enhance photocatalytic performance(Hameed, Gondal, & Yamani, 2004). Moreover, combining Mn–WO_3 with a hydrogel matrix offers further benefits: the hydrogel's porous three-dimensional network boosts pollutant adsorption, ensuring that contaminants are concentrated near the photocatalytic sites. This synergistic effect not only enhances pollutant removal and photocatalytic degradation efficiency but also improves the material's stability and reusability (Ding et al., 2024).The aim of this research is to synthesize hydrogel composites that incorporate manganese-doped tungsten oxide (Mn–WO_3) nanoparticles through a hydrothermal method, followed by crosslinking with sodium alginate and $CaCl_2$. The primary aim is to create and assess a versatile material capable of both adsorbing pollutants and catalyzing their breakdown under solar light exposure. The hydrogel's porous structure is intended to offer a large surface area for adsorption, while the Mn–WO_3 nanoparticles are anticipated to boost photocatalytic efficiency in visible light by narrowing the band gap of WO_3. This integrated strategy provides dual functionalities, adsorption of pollutants and their photocatalytic degradation, presenting an eco-friendly and energy-saving solution for wastewater treatment, with additional prospects for water-splitting applications.

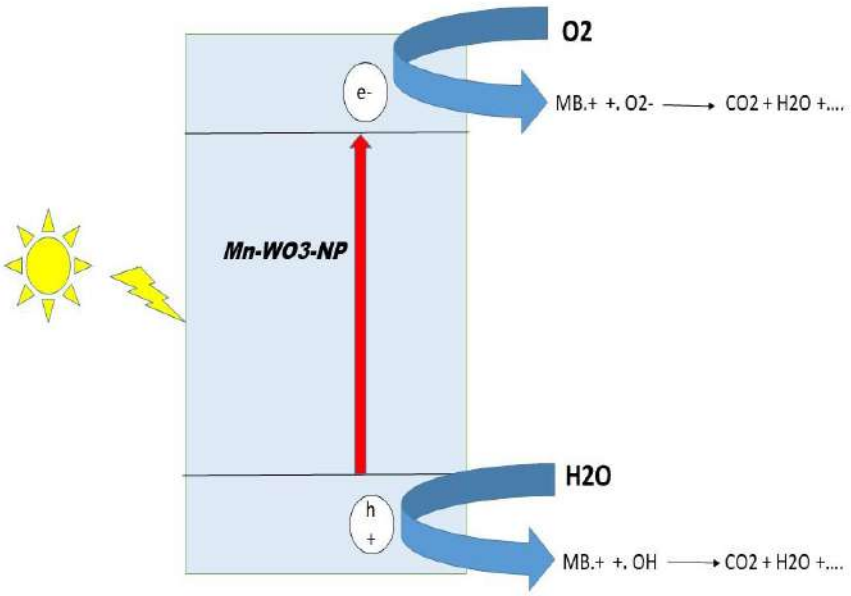

Fig 1: Hydrogels in water decontamination

Method and Material

Synthesis of WO_3 Nano particles

WO3 nanoparticles were synthesized using a direct chemical precipitation approach. Initially, 4.98g of tungstic acid was accurately measured and dissolved in 20ml of a 1M NaOH solution. This mixture was then subjected to continuous stirring on a magnetic stirrer for 2 hours. During this process, white precipitates formed, and the solution was allowed to settle for an additional hour. The supernatant was carefully removed with a pipette, and the precipitates were washed through centrifugation until they turned pale yellow. These precipitates were then transferred to a Petri dish and dried in an oven set at 130°C for 12 hours, resulting in a yellow WO3 powder. This powder was collected with a spatula, finely ground, and placed in a crucible. The crucible was then heated in a
muffle furnace at 600°C for 5 hours. The final product, consisting of pure tungsten oxide nanoparticles, appeared as a white orlight-yellow powder and was stored in sample bottles.

Synthesis of Mn-doped WO3 particles

To synthesize manganese-doped tungsten oxide nanoparticles, 1 g of tungsten oxide nanoparticles was measured using an analytical balance. This was dissolved in 30 ml of water and subjected to continuous stirring with a magnetic stirrer. After one hour of stirring, 3% W/V of the doping agent, manganese chloride, was weighed and added to the reaction mixture, which was then stirred for an additional three hours. The reaction mixture was subsequently transferred to a Teflon-lined stainless-steel autoclave and heated in an oven at 180°C for 24 hours. Upon removal from the autoclave, light brown precipitates were obtained. These precipitates were washed three times with water and ethanol to neutralize them, placed in a petri dish, and dried in an oven at 120°C for five hours. The particles were then collected in a sample bottle for further application.

Synthesis of Mn-doped WO3 NP based Hydrogels

To prepare the composite, 2 g of Mn-WO3 was measured and dissolved into 100 mL of sodium alginate solution, followed by continuous stirring

with a magnetic stirrer for 2 hours to achieve a homogeneous mixture. Calcium chloride (CaCl2) was employed as a crosslinking agent, with a 3% w/v solution of CaCl2 prepared in a beaker and stirred until fully dissolved. Using a 20 mL syringe, the sodium alginate solution containing Mn-doped WO3 particles was incrementally introduced into the CaCl2 solution with continuous stirring. This process resulted in the formation Subsequently, the beads were separated and rinsed with distilled water three times before being processed for further application.

Result and Discussion

Characterization of NP and composite

The synthesized material is exposed to analysis or characterization by using FT-IR for identification of functional groups and XRD examination to assess different essential features (Wang, Liu, Guo, Ge, & Liu, 2021).

FTIR Analysis

The FTIR spectroscopic technique is utilized to identify the functional groups present on the catalyst surface. The FTIR results for the samples are illustrated in Fig 2. As the materials were synthesized via the hydrothermal method, the FTIR spectra of

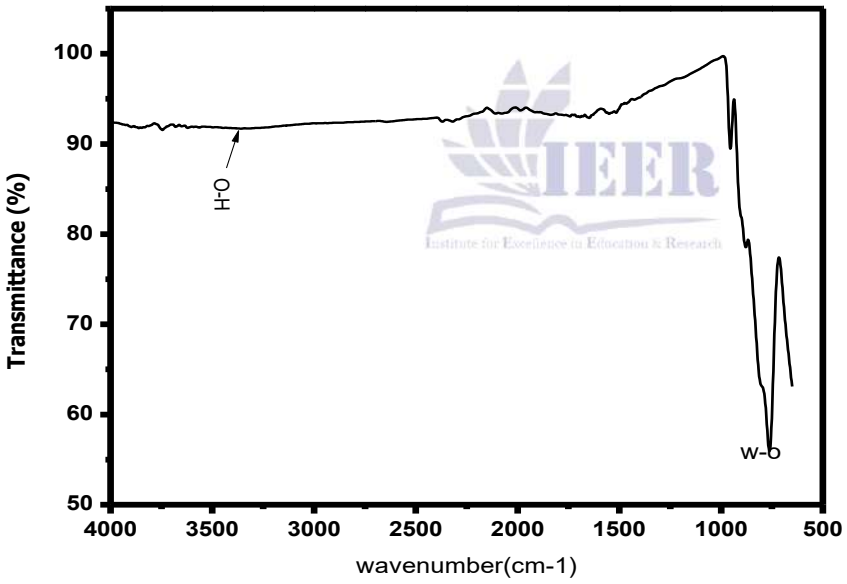

Fig 2: FTIR of pure WO_3 hydrogel

the tungsten oxide nanoparticles are presented in Figure 3. The functional groups
of the materials remained unchanged, as evidenced by the consistent spectrum observed across all three media. A significant peak in the higher frequency region
(approximately 3400 cm-1) indicates the presence of several O–H stretching modes. In all the materials, W–O stretching vibration peaks were identified between 807 and 839 cm-1, confirming the formation of WO3 nanoparticles. Two very weak signals were observed: one at 1631–1641 cm-1, attributed to the bending of an H–O–H coordinated water molecule, and another at 3405 cm-1, indicating the presence of O–H stretching vibrations of coordinated water.

The FTIR spectra of pure and Mn-doped WO3 samples (3 and 10 wt percent) at room temperature

are presented in Figure 3. Table 1 details the observed wave numbers, assignments, and relative intensities derived from the spectra. The tungsten oxide vibrations, corresponding to the W-O stretching, bending, and lattice modes(Krašovec, Vuk, & Orel, 2001), are identified in the infrared region of 1453-600 cm-1. Due to their low absorption characteristics, waves with wave numbers exceeding 3700 cm-1 exhibit very high transmittance. The peak at 1620cm-1 may be attributed to W-OH vibrations. A prominent band associated with the W-O-W bridging mode is observed in the spectrum at 830 cm-1. The Mn-O stretching and bending modes are represented by the bands at 767 and 769 cm-1, respectively (Krašovec et al., 2001). The peaks shifted to higher wave numbers upon Mn doping, which may be attributed to the larger doped samples.

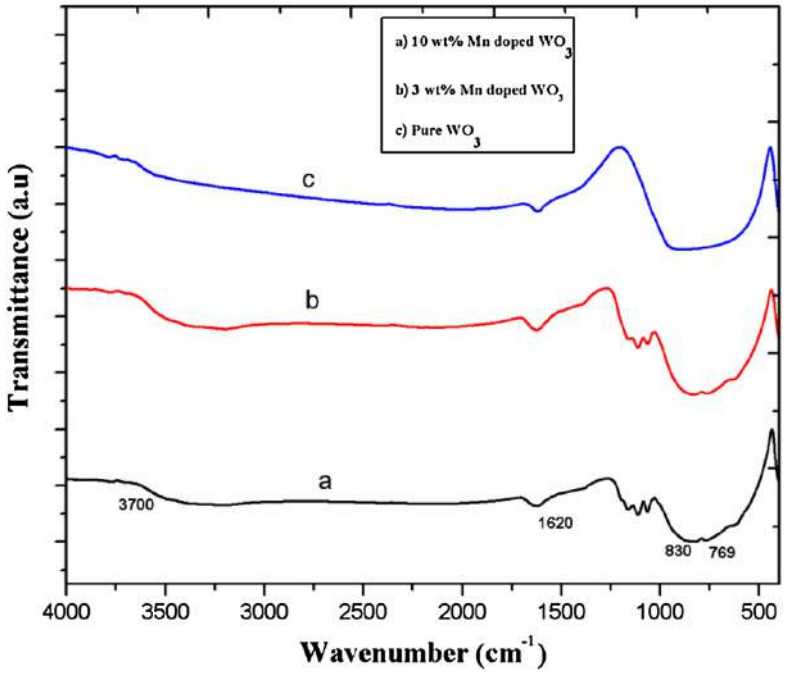

Fig 3: FTIR of pure WO_3 hydrogel and Mn doped WO_3 Hydrogel

UV-visible diffusion reflectance spectroscopy

The diffusion reflectance spectra of pure and Mn-doped WO3 are illustrated in Figures 4a–c, respectively. The absorption edge of the materials corresponds to the shift in the spectrum from 650 to 450 nm towards shorter wavelengths. It is evident from Figures 3b and 3c that the incorporation of manganese into pure WO3 results in an increase in bandgap energy. This phenomenon occurs because the optical transparency of pure WO3 diminishes as Mn doping in WO3 increases. The presence of metal ions (Mn2+) in Mn-doped WO3 leads to a reduction in transmittance and an enhancement in reflectance (Khan et al., 2024). With an increase in Mn content from 0 to 10 wt percent, the bandgap energy for doped samples decreases, and a significant red shift is observed in the absorption edges. The bandgap energies (Eg) have been calculated using the Kubelka–Munk (K–M) model, where the intercept value provides the bandgap energy (Tiwari, Joshi, & Joshi, 2024). The bandgap energies for pure, 3%, and 10% Mn-doped WO3 were calculated. The results indicate

that the bandgap energy decreases with the level of manganese doping.

Table 1 Bandgap energy for pure and Mn doped WO3

Material	Bandgap
Pure WO3	2.91
3% Mn-doped	2.84
10% Mn-doped	2.80

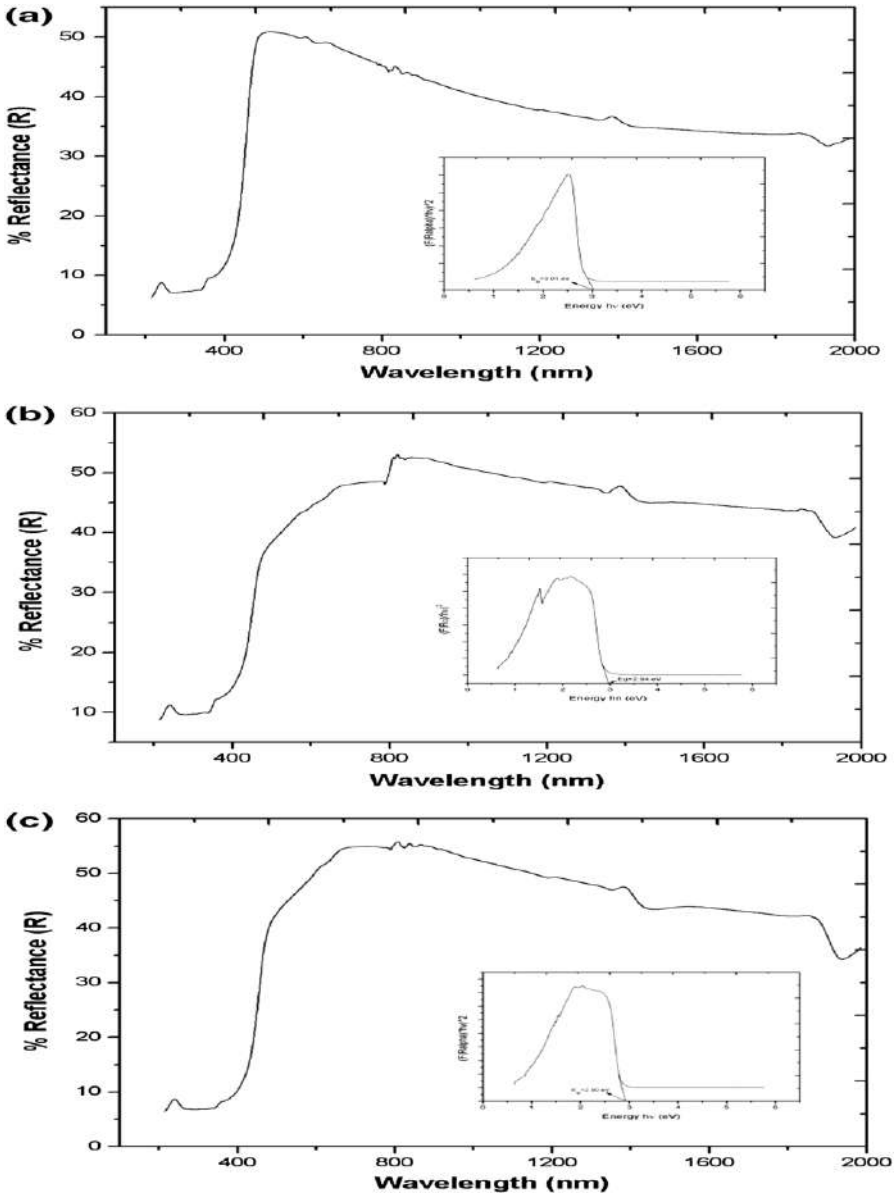

Fig 4: Diffuse reflectance spectra and corresponding bandgap energies of pure and Mn-doped WO_3 samples

XRD Analysis

The phase formation and microstructure of both pure and Mn-doped WO3 are examined using XRD, as depicted in the figure 5. The figure reveals that pure WO3 shows diffraction peaks at 2θ = 23.123, 23.594, and 24.371, corresponding to the (002), (020), and (200) reflections of the monoclinic phase of WO3. The lattice parameters for the synthesized pure and Mn-doped WO3 are a = 7.300, b = 7.538, c = 7.689, and β = 90.892 . In the Mn-doped samples, no secondary phases such as Mn, MnO, or WO3_H_2O are detected, indicating the samples' pure crystallinity. As the Mn concentration increases, the intensity of the peaks decreases. The full width at half maximum (FWHM) of the diffraction peak for WO3 is reduced in Mn-doped WO3, suggesting a decrease in the crystallite size of the Mn-doped WO3. The average crystalline size (D) for both pure and Mn-doped WO3 was determined using Debye–Scherrer's equation (Tiwari et al., 2024).

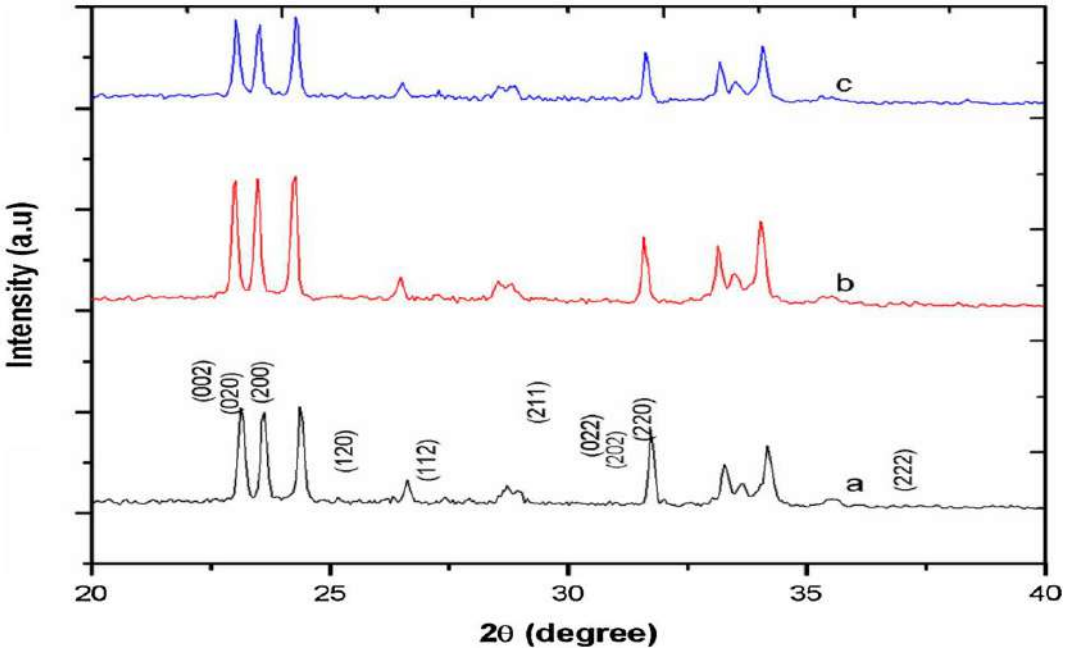

Fig 5: XRD Analysis of pure WO3 hydrogel and Mn doped WO3 Hydrogel

4 Operating Parameters

These five parameters such as pH, Catalyst concentration, Oxidant dose, Irradiation time and Initial dye concentration used for determined the photocatalytic activities of composites

Effect of pH on Photocatalytic Efficiency

pH is one of the key parameters that influences the photocatalytic performance of the material (Alkaim et al., 2014). The photocatalytic activity of Mn-WO3and Mn-WO3/($C_{12}H_{14}CaO_{12}$)n was determined at various pH values
ranging from 2 – 9 (Kanafin, Abduvalov, Kaikanov, Poulopoulos, & Atabaev, 2025). The results are presented in figure which were taken after regular time intervals. The presented data clearly demonstrates that Mn-WO3and Mn-WO3/($C_{12}H_{14}CaO_{12}$)n exhibit their best photocatalytic activity at pH = 3. The catalysts do not degrade methylene blue dye under basic conditions effectively. The photocatalytic efficiency goes on decreasing by increasing the values of pH from acidic to the basic. This can be understood by noticing the value of point of zero charge of the catalyst which happens to be at pH 3, the surface of the catalyst becomes negatively charged which is favorable for the degradation of cationic dyes like methylene blue. Methylene blue gets adsorbed on the catalyst surface due to the negative charge on catalyst surface. When pH moves towards higher basic values, the hydroxyl radicals are scavenged due to which photocatalytic efficiency goes on decreasing (Haleem, Shafiq, Chen,

& Nazar, 2023). Furthermore, sludge is produced by the reaction of excessive ferrous ions and hydroxyl radicals at higher pH values. The active sites of the photocatalyst are blocked by this sludge leading to the decline in photodegradation efficiency(Yildiz & Olabi, 2021).

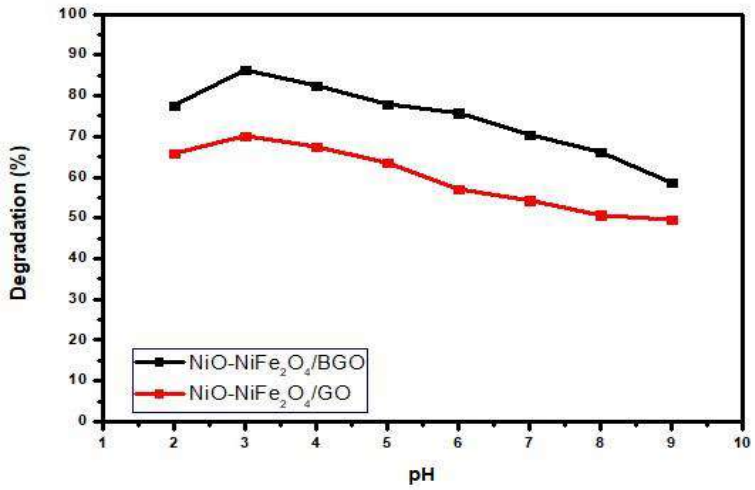

Fig 6: Effect of pH

Effect of Catalyst Concentration on Photocatalytic Efficiency

The concentration of the catalyst is a pivotal factor in determining the photocatalytic performance of semiconductor-based systems, as it directly affects the number of reactive sites available for the adsorption and subsequent degradation of organic pollutants (G. Singh, Ubhi, Jeet, Singla, & Kaur, 2023). This study evaluates varying amounts of Mn-WO_3 and Mn-WO_3/$(C_{12}H_{14}CaO_{12})_n$ to identify the optimal dosage for maximum degradation efficient. The findings indicate that the photocatalytic activity of Mn-WO_3/$(C_{12}H_{14}CaO_{12})_n$ increases steadily as the catalyst concentration is raised from 5 mg/100 mL to 15 mg/100 mL, at which point the highest

degradation rate is achieved. Beyond this concentration, a gradual decline in
photocatalytic efficiency is observed. In contrast, the photocatalytic activity of Mn-WO_3 continues to improve up to 40 mg/100 mL of catalyst, after which the degradation efficiency similarly decreases.
The observed enhancement in efficiency at lower catalyst loadings can be attributed to the increased availability of surface-active sites, which provide more opportunities for dye molecule adsorption. When a larger fraction of the dye molecules interacts with these active
redox reactions increases, resulting in accelerated degradation. Additionally, higher catalyst amounts at this stage promote enhanced generation of reactive oxygen species (ROS), such as hydroxyl (·OH) and superoxide (O_2·$^-$) radicals, which play a dominant role in breaking down the dye molecules (S. Singh, Parveen, Clarizia, & Kumar, 2025). However, this beneficial effect is limited to an optimized catalyst concentration. At higher dosages, several counterproductive phenomena occur. First, the excessive accumulation of nanoparticles promotes agglomeration, leading to a decrease in effective surface area and a reduction in the number of accessible reactive sites. Second, excess catalyst particles increase turbidity and cause significant light scattering and shielding effects. As a result, the penetration of solar light to deeper layers of the suspension is obstructed, and insufficient photon energy reaches the semiconductor surface. This reduces the efficiency of electron excitation from the valence band (VB) to the conduction band (CB), thereby lowering the generation of electron–hole pairs essential for photocatalytic reactions (Rafiq et al., 2021). Furthermore, the recombination rate of photogenerated charge carriers may increase under

such conditions, further diminishing the overall activity.

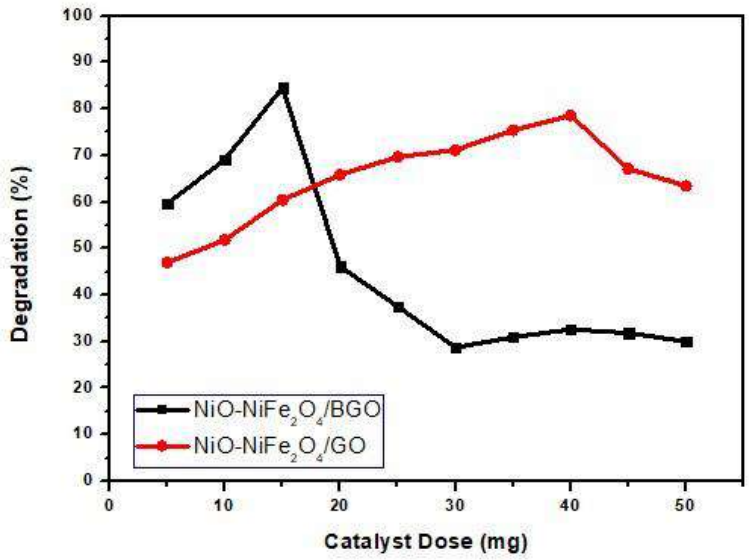

Fig 7 : Effect of Catalyst concentration

Effect of Oxidant Dose on Photocatalytic Efficiency

After optimizing pH and catalyst concentration, the oxidant dose was optimized by using different concentrations of hydrogen peroxide ranging from 3 mM to 15 mM/100 mL of dye solution. The photocatalytic efficiency of Mn-WO_3 and Mn-$WO_3/(C_{12}H_{14}CaO_{12})_n$ was evaluated at consistent intervals, with the results presented in graph. Both catalysts exhibited a gradual increase in degradation efficiency as the H_2O_2

concentration rose. A graph was obtained after getting experimental results after fixed time intervals. These results are depicted in figure 8. By examining the results, it can be said that the photocatalytic efficiency of the catalyst increases with increase in the concentration of the oxidant up to a certain value. This increase in efficiency is accredited to the increase in the number of active degrading hydroxyl radicals which are involved in the mineralization of the organic dye molecules (D. Chen et al., 2020). The photocatalytic activity of Mn-WO3/(C12H14CaO12)n and Mn-WO3continues to increase until oxidant dose of 11 mM/100 mL of the dye solution and then decrease onwards. The reason behind this increase is mentioned earlier in this section. Moreover, hydroxyl radicals are also involved in charge separation as they can accept electrons from the conduction band (Al Miad et al., 2024). Hydrogen peroxide accepts electron from superoxide radical to generate hydroxyl radicals.

$$H_2O_2 + O^{2-} \rightarrow HO^- + HO^\cdot + O_2$$

$$H_2O_2 + e^-_{(CB)} \rightarrow HO^- + HO^\cdot$$

After a certain limit, the photocatalytic efficiency starts to decrease by further increasing oxidant dose. This is ascribed to the generation of hydrogen peroxide radicals which are not only less reactive than hydroxyl radicals but also scavenge them (Atharizade & Miranzadeh, 2015).

$$H_2O_2 + HO^\cdot \rightarrow H_2O + HO^\cdot$$

$$HO^-_2 + HO^\cdot \rightarrow H_2O + O_2$$

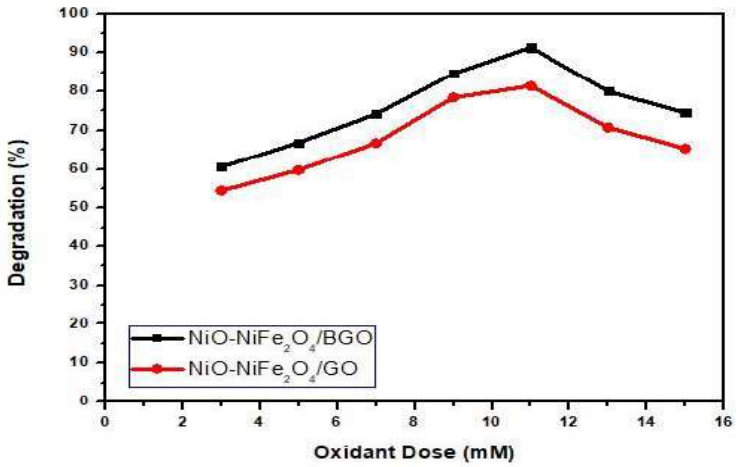

Fig 8 : Effect of Oxidant Dose

Effect of Irradiation Time on Photocatalytic Degradation

Time to attain the maximum degradation of methylene blue was determined by keeping the other parameters like pH, catalyst concentration, and oxidant dose constant. Samples were taken from the reaction mixture at regular intervals, and the remaining dye concentration was measured using a UV–Visible spectrophotometer. The reaction was carried under the time range of 10-140 minutes and the results were plotted as shown in figure.

The degradation efficiency consistently improved with increased irradiation time, achieving a maximum photocatalytic activity of over 92% for Mn-WO_3/$(C_{12}H_{14}CaO_{12})_n$ at 100 minutes and more than 82% for Mn-WO_3 at 120 minutes. After these points, the degradation curves leveled off, indicating no further significant decrease in dye concentration.

The initial rapid degradation phase is due to the plentiful active sites and reactive oxygen species (·OH and $O_2{\cdot}^-$) that attack the dye molecules. As the reaction progresses, the methylene blue concentration diminishes, leaving fewer molecules available for adsorption on the catalyst surface, which slows the degradation rate (Yin, Liu, & Ai, 2021). The degradation efficiency consistently increased with increased irradiation time, reaching at approximately 92% for Mn-WO_3/$(C_{12}H_{14}CaO_{12})_n$ after 100 minutes and around 82% for Mn-WO_3 after 120 minutes after which the curves levelled off, indicating equilibrium between ROS generation and remaining dye molecules (Tsaviv et al., 2024).

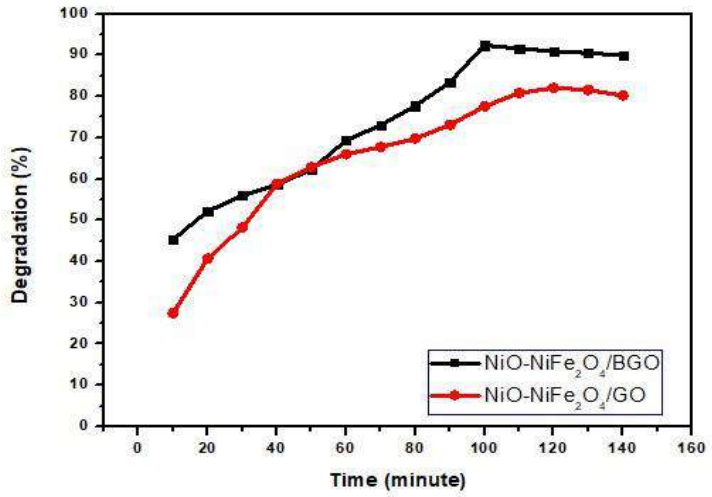

Fig 9: Effect of time

Radical Scavenging Experiment and Proposed Degradation Mechanism

Hydroxyl radicals, holes, and electrons constitute the reactive species involved in the photocatalytic degradation of dyes and other organic contaminants(Naseem et al.) To assess the efficiency of these reactive species, specific scavengers are introduced into the reaction mixture. Dimethyl sulfoxide (DMSO) serves as a scavenger for hydroxyl radicals, ethylenediamine tetraacetate (EDTA) for holes, and potassium dichromate (K2Cr2O7) for electrons (Tabasum et al., 2020). The reaction is conducted under previously optimized conditions, including pH, catalyst concentration, oxidant dose, and time. A 5 mL aliquot of a 5 mM solution of each scavenger is added to the reaction mixture, and their impact on the efficiency of their respective target species is evaluated. The results from the scavenger study are illustrated in the accompanying figure 10. It is evident that DMSO significantly reduces the photocatalytic efficiency of NiO-NiFe2O4/BGO, with approximately a 65% decrease in the degradation of methylene blue, indicating that hydroxyl radicals are the primary species responsible for photocatalytic

degradation. Conversely, the reductions in efficiency due to EDTA and potassium dichromate are approximately 45% and 27%, respectively. Consequently, it can be concluded that hydroxyl radicals are the principal agents in the photocatalytic degradation process, with a minor contribution from holes, followed by electrons.

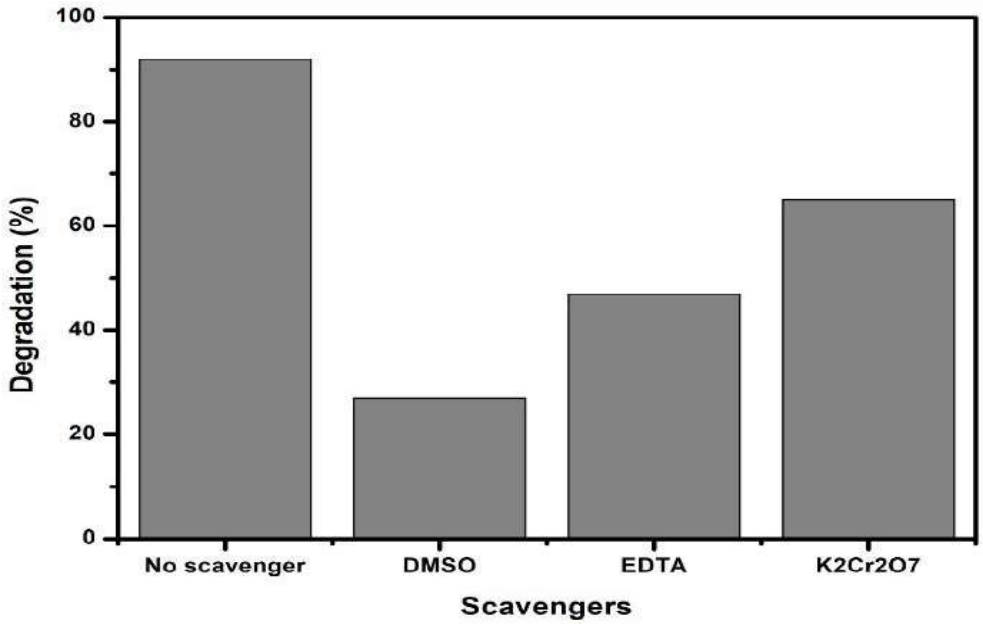

Fig 10: Effect of different scavengers on the photocatalytic activity of of Mn-WO3

Reusability test

Another advantage associated with heterogeneous photocatalysis is the easy separation of photocatalyst from the reaction mixture and its reusability for another degradation reaction for many cycles. The stability test was conducted by performing the degradation experiment across three cycles (Palharim et al., 2024). Following each cycle,the photocatalyst was separated from the reaction mixture via ultracentrifugation, washed with distilled water, dried, reweighed, and subsequently reused in the next cycle. The degradation efficiency of Mn-WO3/(C12H14CaO12)n decreased from over 92% to approximately 82% after three consecutive cycles, as illustrated in the figure 11. These reusability results indicate the good stability of Mn-WO3/(C12H14CaO12)n after three cycles. Furthermore, the slight reduction in photocatalytic efficiency may be attributed to the decline or blockage of active sites on the catalyst surface after multiple cycles (Mukonza, Chaukura, & Mishra, 2022)

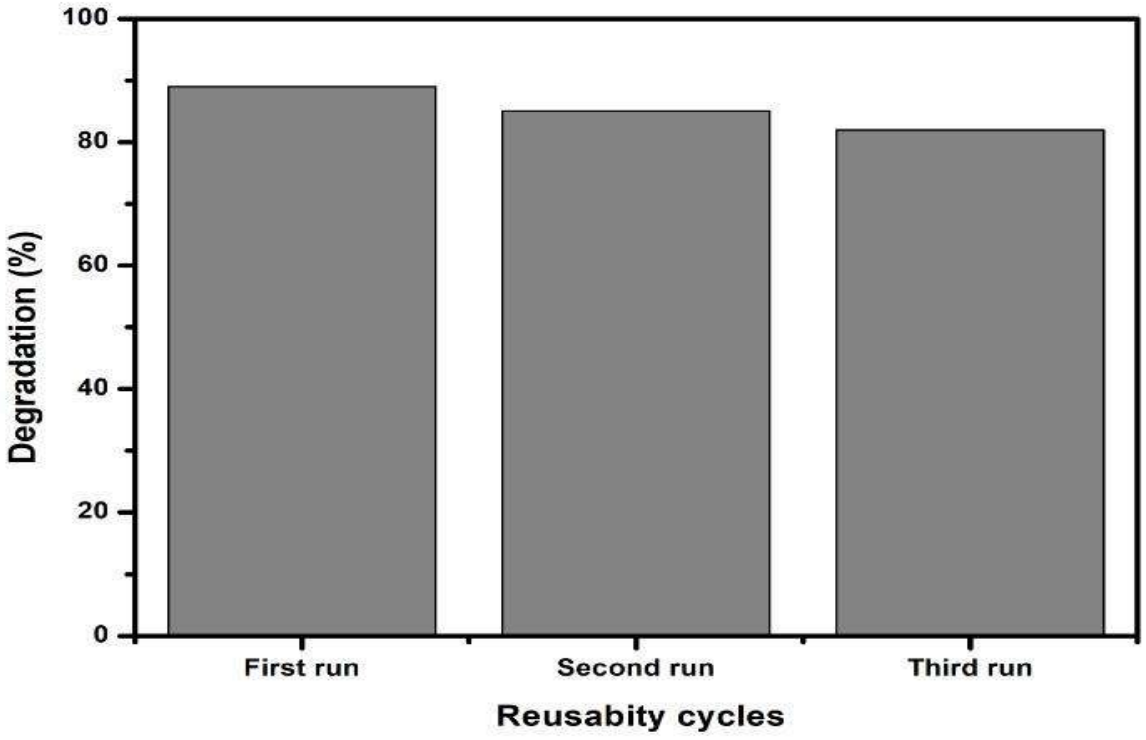

Fig 11: Photocatalytic degradation results of methylene blue by Mn-WO3/(C12H14CaO12)nfor three reusability runs.

4.5 Reaction Kinetics

pseudo-first-order and pseudo-second-order models to the experimental data .The equations for these models are given below (Lin & Wang, 2009).

ln Co / Ct = K1t (first order)
1 / Ct – 1
/ Co = K2
second o
rder

Here, "Co" represents initial concentration of dye solution at time zero and "Ct" at the specific time denoted by "t" (Fan et al., 2015). "K1" and "K2" stand for the rate constant of first and second order reaction, respectively. A linear relation between "ln Co / Ct" and time indicates first-order kinetics, from which the slope yields the rate constant K1. Similarly, the plot between "1 / Ct – 1 / Co" and time also results in a linear relation and the slope of this plot gives the value of K2, the rate constant for the second order reaction (Fan, Li, Evans, & Duan, 2014).

A comparison of correlation coefficients (R^2) revealed that the pseudo-first-order model exhibited a superior fit to the experimental data compared with the pseudo-second-order model, indicating that the photocatalytic degradation process follows pseudo-first-order kinetics under the studied conditions (Tran, Nguyen, Do, & Tran, 2023).The calculated rate constant (K1) for Mn-WO_3/$(C_{12}H_{14}CaO_{12})_n$ was several times higher than that of NiO–$NiFe_2O_4$/GO, confirming its superior photocatalytic activity. The enhancement can be attributed to the synergistic effects of boron doping and the hydrogel matrix, which facilitate efficient charge carrier separation, suppress electron-hole recombination, and promote the generation of reactive oxygen species. Consequently, Mn-WO_3/$(C_{12}H_{14}CaO_{12})_n$ exhibits accelerated degradation kinetics and enhanced photocatalytic efficiency compared with the reference catalyst.

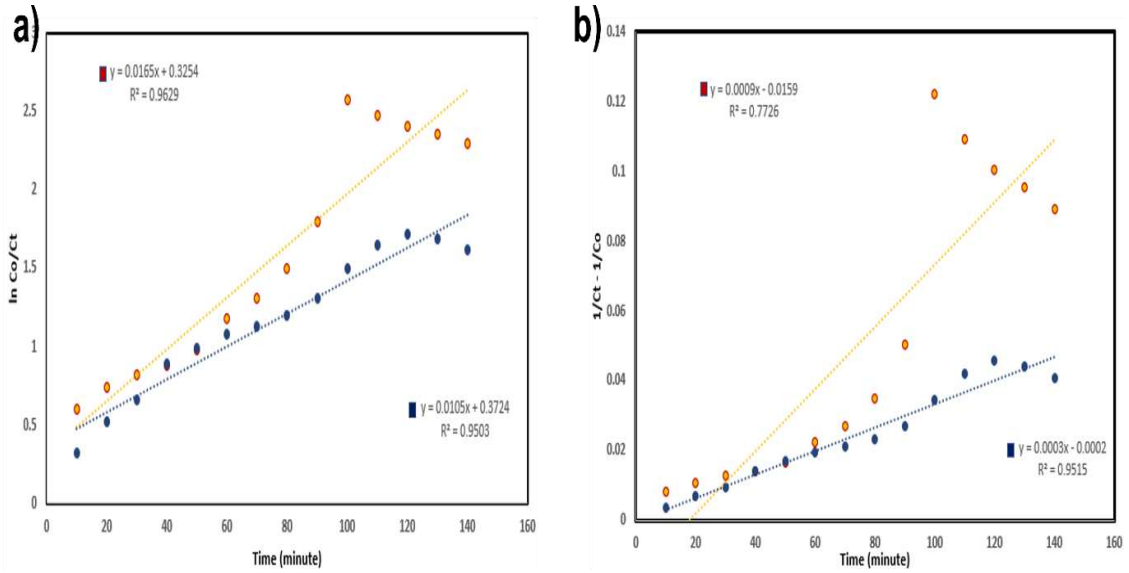

Fig 12 : Reaction kinetics (a) 1st order kinetics model, (b) 2nd order kinetics model for the degradation of methylene blue by of Mn-WO3.

The Combined Influence of Operating Parameters

The combined impact of pH and catalyst dosage on the photocatalytic breakdown of methylene blue was examined, with findings displayed in Figure 13. Both contour and three-dimensional (3D) surface plots were created to demonstrate the interactive effects of these parameters. The study was carried out within a pH range of 2–4 and a catalyst loading of 10–20 mg per 100 mL of dye solution. It was noted that the degradation efficiency improved as the pH increased from 2 to 3, but then declined beyond this point. The initial enhancement in performance is due to improved surface charge interactions between the photocatalyst and dye molecules, which promote the adsorption of methylene blue. However, at higher pH levels, the excess hydroxide ions in the medium tend to scavenge photo-generated holes, thereby inhibiting hydroxyl radical formation and decreasing the overall degradation efficiency (Rodríguez-Chueca, Carbajo, & García-Muñoz, 2023). A similar pattern was observed with changes in catalyst concentration.

The degradation efficiency consistently increased as the catalyst loading rose from 10 mg to 15 mg per 100 mL, attributed to the greater number of active sites and the larger surface area available for light absorption and pollutant interaction. Beyond this optimal level, a gradual reduction in photocatalytic activity was observed. This decline is mainly due to nanoparticle agglomeration, which reduces the effective surface area and causes partial light scattering, thus hindering the penetration of photons to the catalyst surface. The blockage of active sites further limits the generation of reactive oxygen species (ROS), leading to reduced photocatalytic efficiency under solar irradiation (Mohammadi-Galangash, Mousavi, & Shirzad-Siboni, 2025). The combined effect of pH and oxidant dose is shown in Figure 4.15b, where the oxidant concentration was varied between 9 mM and 13 mM. The photocatalytic efficiency increased with rising oxidant concentration up to an optimum of 11 mM, after which a decline was noted. This behavior can be explained by the enhanced production of hydroxyl radicals (·OH) with increasing hydrogen peroxide concentration up to the optimum level (Rodríguez-Chueca et al., 2023). However, at higher concentrations, excess H_2O_2 undergoes self-scavenging or reacts with ·OH to form less reactive hydroperoxyl radicals (HO_2·), thus diminishing the degradation rate (Rosa, Lattanzio, Bavasso, & Di Palma, 2023).The interactive relationship between catalyst concentration and oxidant dose is depicted in Figure 13c Maximum degradation efficiency was achieved at optimized values of 15 mg per 100 mL catalyst loading and 11

mM oxidant dose. Beyond these levels, the degradation percentage decreased due to a combination of factors: agglomeration of catalyst particles at higher loadings and the formation of excess hydrogen peroxide species that act as radical scavengers rather than promoters. These results confirm that an optimal balance between catalyst amount and oxidant concentration is essential to achieve maximum photocatalytic performance (Ibhadon & Fitzpatrick, 2013).

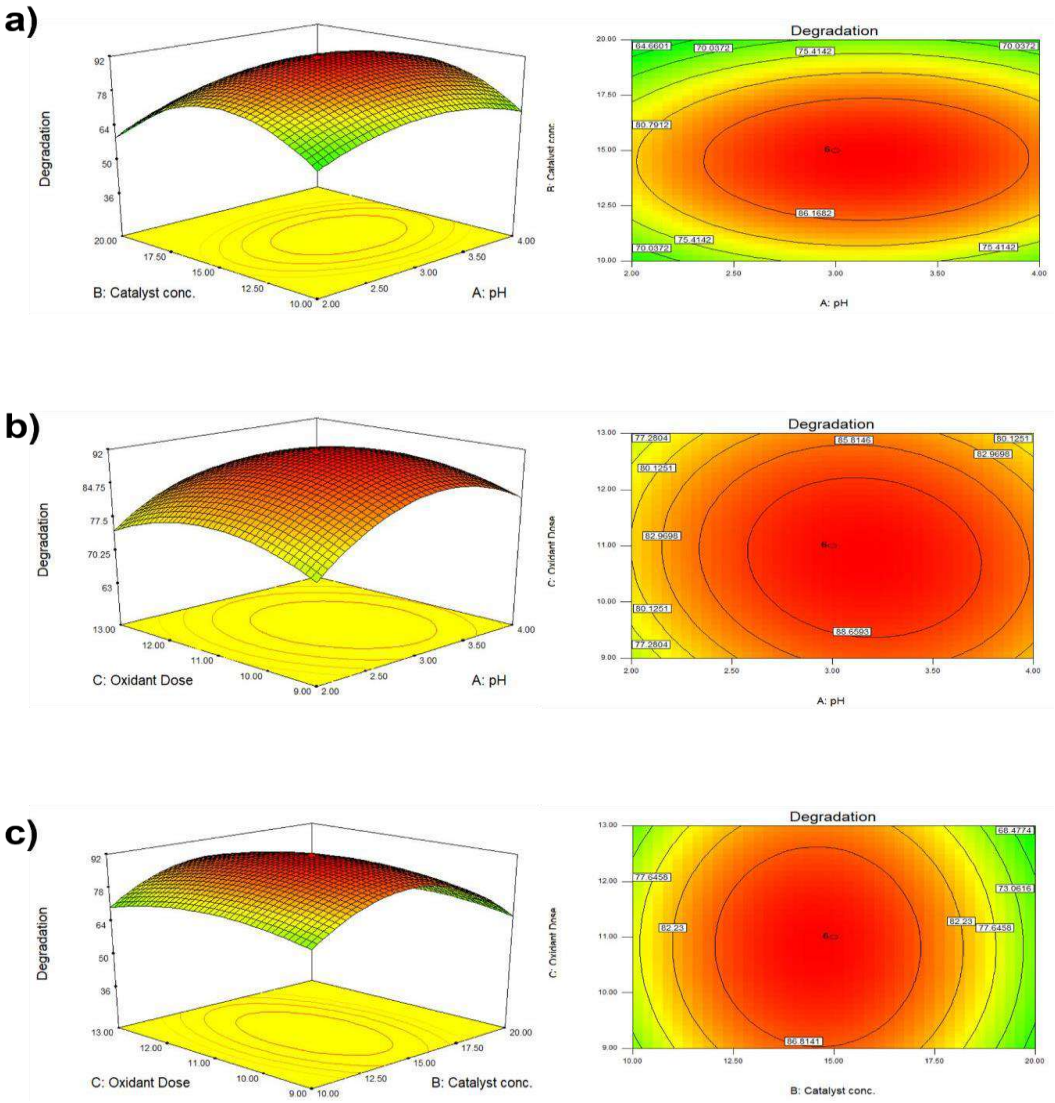

Fig 13 : Response Surface Methodology, 3D and contour graphs showing mutual interaction between (a) pH and catalyst concentration, (b) pH and oxidant dose, and (c) catalyst concentration and oxidant dose.

Conclusion

This research successfully synthesized Mn-doped WO_3 and Mn-WO_3/$(C_{12}H_{14}CaO_{12})_n$ hydrogel composites, showcasing improved photocatalytic efficiency for methylene blue degradation under visible light. The hydrothermal synthesis technique ensured uniform Mn integration into the WO_3 lattice, preserving its monoclinic structure and reducing the bandgap from 2.91 to 2.80 eV. Detailed

characterization using FTIR, XRD, SEM/EDX, and UV–Vis DRS confirmed the structural modifications and enhanced light absorption. The inclusion of boron-doped graphene oxide further boosted charge transfer and surface activity, leading to superior photocatalytic performance. Under optimal conditions (pH 3, catalyst loading of 15–40 mg/100 mL, oxidant dose of 11 mM, and irradiation time of 100–120 min), the Mn-WO_3/$(C_{12}H_{14}CaO_{12})_n$ composite achieved nearly 95% degradation efficiency. Kinetic studies revealed pseudo-first-order behavior, with hydroxyl radicals identified as the main reactive species in dye degradation. The improved separation of charge carriers between Mn-WO_3 and boron-doped graphene oxide contributed to the enhanced visible-light response and reduced recombination rate. The catalyst demonstrated excellent stability and reusability, maintaining high activity over three cycles, indicating its potential for long-term use. Statistical optimization via Response Surface Methodology (RSM) confirmed the system's robustness and consistency across different operating conditions. In summary, the Mn-WO_3/$(C_{12}H_{14}CaO_{12})_n$ hydrogel composite is an efficient, durable, and environmentally friendly photocatalyst for wastewater treatment, with promising applications in energy conversion, catalytic systems, and environmental protection technologies.

REFERENCE

Al-Rasheed, R. A. (2005). *Water treatment by heterogeneous photocatalysis an overview*. Paper presented at the Fourth SWCC Acquired Experience Symposium.

Al Miad, A., Saikat, S. P., Alam, M. K., Hossain, M. S., Bahadur, N. M., & Ahmed, S. (2024). Metal oxide-based photocatalysts for the efficient degradation of organic pollutants for a sustainable environment: a review. *Nanoscale Advances*, *6*(19), 4781-4803.

Alkaim, A., Aljeboree, A., Alrazaq, N., Baqir, S., Hussein, F., & Lilo, A. (2014). Effect of pH on adsorption and photocatalytic degradation efficiency of different catalysts on removal of methylene blue. *Asian Journal of Chemistry*, *26*(24), 8445.

Archana, C., Kanakalakshmi, A., Nithya, K., Kaarunya, E., & Renugadevi, K. (2025). Health Effects of Emerging Contaminants: Effects on Humans Via Ingestion of Contaminated Water *Emerging Contaminants in Water* (pp. 269-306): Springer.

Atharizade, M., & Miranzadeh, M. B. (2015). Evaluation of efficacy of advanced oxidation processes fenton, fenton-like and photo-fenton for removal of phenol from aqueous solutions. *J Chem Soc Pak*, *37*(02), 266.

Baggio, G., Qadir, M., & Smakhtin, V. (2021). Freshwater availability status across countries for human and ecosystem needs. *Sci Total Environ*, *792*, 148230. doi:10.1016/j.scitotenv.2021.148230

Bermúdez, L. A., Pascual, J. M., Martínez, M. d. M. M., & Poyatos Capilla, J. M. (2021). Effectiveness of advanced oxidation processes in wastewater treatment: State of the art. *Water*, *13*(15), 2094.

Chen, D., Cheng, Y., Zhou, N., Chen, P., Wang, Y., Li, K., . . . Zhang, R. (2020). Photocatalytic degradation of organic pollutants using TiO2-based photocatalysts: A review. *Journal of Cleaner Production*, *268*, 121725.

Chen, S., Hu, Y., Meng, S., & Fu, X. (2014). Study on the separation mechanisms of photogenerated electrons and holes for composite photocatalysts g-C3N4-WO3. *Applied Catalysis B: Environmental*, *150*, 564-573.

Ding, J., Yang, Y., Poisson, J., He, Y., Zhang, H., Zhang, Y., . . . Zhang, K. (2024). Recent advances in biopolymer-based hydrogel electrolytes for flexible supercapacitors. *ACS Energy Letters*, *9*(4), 1803-1825.

Dutta, S., Adhikary, S., Bhattacharya, S., Roy, D., Chatterjee, S., Chakraborty, A., . . . Rajak, P. (2024). Contamination of textile dyes in aquatic environment: Adverse impacts on aquatic ecosystem and human health, and its management using bioremediation. *Journal of Environmental Management*, *353*, 120103.

Fan, G., Li, F., Evans, D. G., & Duan, X. (2014). Catalytic applications of layered double hydroxides: recent advances and perspectives. *Chemical Society Reviews*, *43*(20), 7040-7066.

Fernandes, J., Ramísio, P. J., & Puga, H. (2024). A comprehensive review on various phases of wastewater technologies: Trends and future perspectives. *Eng*, *5*(4), 2633-2661.

Gisbertz, S., & Pieber, B. (2020). Heterogeneous photocatalysis in organic synthesis. *ChemPhotoChem*, *4*(7), 456-475.

Guglielmi, G. (2017). Arsenic in drinking water threatens up to 60 million in Pakistan. *Science*, *24*(2017), 15-16.

Haleem, A., Shafiq, A., Chen, S.-Q., & Nazar, M. (2023). A comprehensive review on adsorption, photocatalytic and chemical degradation of dyes and nitro-compounds over different kinds of porous and composite materials. *Molecules*, *28*(3), 1081.

Hameed, A., Gondal, M., & Yamani, Z. (2004). Effect of transition metal doping on photocatalytic activity of WO3 for water splitting under laser illumination: role of 3d-orbitals. *Catalysis Communications*, *5*(11), 715-719.

Hoffmann, M. R., Martin, S. T., Choi, W., & Bahnemann, D. W. (1995). Environmental applications of semiconductor photocatalysis. *Chemical reviews*, *95*(1), 69-96.

Hung, W.-H., Peng, C.-J., Yang, C.-R., Li, C.-J., Shyue, J.-J., Chang, P.-C., . . . Juan, P.-C. (2016). Exploitation of a spontaneous spatial charge separation effect in plasmonic polyhedral α-Fe2O3 nanocrystal photoelectrodes for hydrogen production. *Nano energy*, *30*, 523-530.

Ibhadon, A. O., & Fitzpatrick, P. (2013). Heterogeneous photocatalysis: recent advances and applications. *Catalysts*, *3*(1), 189-218.

Kanafin, Y. N., Abduvalov, A., Kaikanov, M., Poulopoulos, S. G., & Atabaev, T. S. (2025). A review on WO3 photocatalysis used for wastewater treatment and pesticide degradation. *Heliyon*, *11*(1).

Khan, M. M., Pawar, M., Ansari, A. A., Ahamed, M., Kumar, S., & Shahabuddin, M. (2024). Boosted photocatalytic and electrochemical activity of hydrothermally synthesized WO3 nanoparticles co-doped with transition elements (Mn, Co). *Materials Science and Engineering: B*, *307*, 117541.

Krašovec, U. O., Vuk, A. Š., & Orel, B. (2001). IR Spectroscopic studies of charged–discharged crystalline WO3 films. *Electrochimica Acta*, *46*(13-14), 1921-1929.

Lam, S.-M., Sin, J.-C., Abdullah, A. Z., & Mohamed, A. R. (2012). Degradation of wastewaters containing organic dyes photocatalysed by zinc oxide: a review. *Desalination and Water Treatment*, *41*(1-3), 131-169.

Lellis, B., Fávaro-Polonio, C. Z., Pamphile, J. A., & Polonio, J. C. (2019). Effects of textile dyes on health and the environment and bioremediation potential of living organisms. *Biotechnology Research and Innovation*, *3*(2), 275-290.

Lin, J., & Wang, L. (2009). Comparison between linear and non-linear forms of pseudo-first-order and pseudo-second-order adsorption kinetic models for the removal of methylene blue by activated carbon. *Frontiers of Environmental Science & Engineering in China*, *3*(3), 320-324.

Mohammadi-Galangash, M., Mousavi, S.-K., & Shirzad-Siboni, M. (2025). Photocatalytic degradation of reactive black 5 from synthetic and real wastewater under visible light with TiO2 coated PET photocatalysts. *Scientific Reports*, *15*(1), 14314.

Mu, R., Liu, B., Chen, X., Wang, N., & Yang, J. (2020). Hydrogel adsorbent in industrial wastewater treatment and ecological environment protection. *Environmental Technology & Innovation*, *20*, 101107.

Mukonza, S. S., Chaukura, N., & Mishra, A. K. (2022). Photocatalytic activity and reusability of F, Sm3+ Co-doped TiO2/MWCNTs hybrid heterostructure for efficient photocatalytic degradation of brilliant black bis-azo dye. *Catalysts*, *13*(1), 86.

Naseem, A., Nadeem, N., Noreen, S., Youssef, M., Rehan, Z., Ali, H., . . . Zahid, M. Sunlight-activated photocatalytic efficiency of novel Zr-CoS-PTh composite for superior wastewater remediation.

Nawaz, A., Zahid, M., Rehman, A., Mansha, A., & Hussain, T. (2023). Sustainable hydrogels as an emerging material platform for water purification *Sustainable Hydrogels* (pp. 375-395): Elsevier.

Nishimoto, S., Mano, T., Kameshima, Y., & Miyake, M. (2010). Photocatalytic water treatment over WO3 under visible light irradiation combined with ozonation. *Chemical Physics Letters, 500*(1-3), 86-89.

Oller, I., Malato, S., & Sánchez-Pérez, J. (2011). Combination of advanced oxidation processes and biological treatments for wastewater decontamination—a review. *Science of the total environment, 409*(20), 4141-4166.

Palharim, P. H., Caira, M. C. D. A., Gusmão, C., Ramos, B., da Câmara, A. G., Pacheco, J. G. A., . . . Teixeira, A. C. S. C. (2024). Enhanced photocatalytic activity and stability of WO3-AgCl/Ag composites: surface modulation by structure-directing agents for effective sunlight treatment of pharmaceutical wastewater. *Journal of Photochemistry and Photobiology A: Chemistry, 450*, 115433.

Pandey, A. K. (2025). Sustainable water management through integrated technologies and circular resource recovery. *Environmental Science: Water Research & Technology, 11*(8), 1822-1846.

Ponnusami, A. B., Sinha, S., Ashokan, H., Paul, M. V., Hariharan, S. P., Arun, J., . . . Pugazhendhi, A. (2023). Advanced oxidation process (AOP) combined biological process for wastewater treatment: A review on advancements, feasibility and practicability of combined techniques. *Environmental research, 237*, 116944.

Rafiq, A., Ikram, M., Ali, S., Niaz, F., Khan, M., Khan, Q., & Maqbool, M. (2021). Photocatalytic degradation of dyes using semiconductor photocatalysts to clean industrial water pollution. *Journal of Industrial and Engineering Chemistry, 97*, 111-128.

Rodríguez-Chueca, J., Carbajo, J., & García-Muñoz, P. (2023). Intensification of photo-assisted advanced oxidation processes for water treatment: a critical review. *Catalysts, 13*(2), 401.

Rosa, D., Lattanzio, S., Bavasso, I., & Di Palma, L. (2023). Investigation of the synergistic effect of hydrogen peroxide and ultrasound on the photocatalytic treatment under visible light of dyes wastewater. *Chemical Engineering Science, 282*, 119290.

Sayed Abhudhahir, M. H., & Kandasamy, J. (2015). Photocatalytic effect of manganese doped WO3 and the effect of dopants on degradation of methylene blue. *Journal of Materials Science: Materials in Electronics, 26*(11), 8307-8314.

Sharma, J., Sharma, S., & Soni, V. (2021). Classification and impact of synthetic textile dyes on Aquatic Flora: A review. *Regional Studies in Marine Science, 45*, 101802.

Silva, J. A. (2023). Wastewater treatment and reuse for sustainable water resources management: a systematic literature review. *Sustainability, 15*(14), 10940.

Singh, G., Ubhi, M. K., Jeet, K., Singla, C., & Kaur, M. (2023). A review on impacting parameters for photocatalytic degradation of organic effluents by ferrites and their nanocomposites. *Processes, 11*(6), 1727.

Singh, S., Parveen, S., Clarizia, L., & Kumar, P. (2025). An insight into photo-catalytic degradation mechanism of persistent pollutants with transition metal oxides and their composites: Photocatalysis mechanism, rate affecting parameters, and removal pathways. *Catalysis Reviews*, 1-49.

Tabasum, A., Alghuthaymi, M., Qazi, U. Y., Shahid, I., Abbas, Q., Javaid, R., . . . Zahid, M. (2020). UV-accelerated photocatalytic degradation of pesticide over magnetite and cobalt ferrite decorated graphene oxide composite. *Plants, 10*(1), 6.

Thangavel, S., Elayaperumal, M., & Venugopal, G. (2012). Synthesis and properties of tungsten oxide and reduced graphene oxide nanocomposites. *Materials Express, 2*(4), 327-334.

Tiwari, M., Joshi, G., & Joshi, A. (2024). Structural and optical investigations of starch-assisted Mn-Doped WO3 nanoparticles for photocatalytic degradation of dyes. *Materials Research Innovations, 28*(2), 120-135.

Tran, H. D., Nguyen, D. Q., Do, P. T., & Tran, U. N. (2023). Kinetics of photocatalytic degradation of organic compounds: a mini-review and new approach. *RSC advances, 13*(25), 16915-16925.

Tsaviv, J., Eneji, I., Sha'Ato, R., Ahemen, I., Jubu, P., & Yusof, Y. (2024). Photodegradation, kinetics and non-linear error functions of methylene blue dye using SrZrO3 perovskite photocatalyst. *Heliyon, 10*(14).

Wang, X., Liu, Z., Guo, Z., Ge, L., & Liu, Z. (2021). NiO–CoFe 2 O 4 electrocatalyst prepared on Ni foam by one-step hydrothermal method for efficient overall water splitting. *Journal of Materials Science*, 1-13.

Yildiz, S., & Olabi, A. (2021). Application of photocatalysis methods to enhance sludge disintegration. *Waste and Biomass Valorization, 12*(8), 4419-4431.

Yin, X., Liu, L., & Ai, F. (2021). Enhanced photocatalytic degradation of methylene blue by WO3 nanoparticles under NIR light irradiation. *Frontiers in chemistry, 9*, 683765.

Zhang, Z., Fu, H., Li, Z., Huang, J., Xu, Z., Lai, Y., . . . Zhang, S. (2022). Hydrogel materials for sustainable water resources harvesting & treatment: synthesis, mechanism and applications. *Chemical Engineering Journal*, 135756.

Zhou, X., Guo, Y., Zhao, F., & Yu, G. (2019). Hydrogels as an emerging material platform for solar water purification. *Accounts of chemical research, 52*(11), 3244-3253.